

## Cation Effects in p-Type Dye-Sensitized Solar Cells

Shannon M. McCullough,<sup>‡</sup> Jake M. Evans,<sup>‡</sup> Taylor Moot, Aaron D. Taggart, Ludovic Troian-Gautier, and James F. Cahoon\*Cite This: *ACS Appl. Energy Mater.* 2020, 3, 1496–1505

Read Online

ACCESS |



Metrics &amp; More

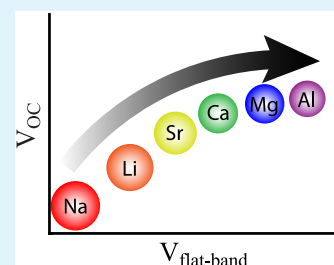


Article Recommendations



Supporting Information

**ABSTRACT:** The performance of dye-sensitized solar cells (DSSCs) depends on the properties and interactions of three fundamental components: the semiconductor, chromophore, and electrolyte. For the electrolyte, the dependence of DSSC performance on the identity and valence state of the spectator cation has not been well studied in p-type semiconductor systems, although the effects of these species in n-type TiO<sub>2</sub> devices are significant, producing large shifts in semiconductor flat-band potential, charge-transfer kinetics, photocurrent, and open-circuit voltage ( $V_{OC}$ ). Here, we vary the spectator cation in p-type NiO DSSCs and demonstrate an increase in  $V_{OC}$  by over 50% with two common redox couples. Using optimal cations, we achieved high  $V_{OC}$  values without a significant reduction in photocurrent. Mott–Schottky analysis and electrochemical impedance spectroscopy reveal that the cation can shift the flat-band potential of NiO by nearly 1 V and substantially alter the lifetime of charge carriers and charge-transfer resistance at the semiconductor–electrolyte interface. Differences between the anionic and cationic redox couples employed suggest favorable and unfavorable interactions, respectively, with divalent cations at the NiO surface, causing increases and decreases in charge carrier recombination rate constants. Our results highlight the complex interaction between the semiconductor and electrolyte solution and indicate that varying the cation should yield immediate improvements in device metrics for most p-type DSSC systems.



**KEYWORDS:** cation effects, dye-sensitized solar cell, nickel oxide, p-type semiconductor, metal oxide, electrolyte

## 1. INTRODUCTION

Dye-sensitized solar cells (DSSCs) are a potential low-cost alternative to traditional silicon solar cells,<sup>1</sup> and the basic components include a semiconductor, a chromophore, and an electrolyte containing a redox couple. Upon illumination, the photoexcited chromophore transfers a hole (electron) to the p-type (n-type) semiconductor, typically the metal oxides NiO and TiO<sub>2</sub> for p- and n-type devices, respectively.<sup>2–6</sup> The chromophore subsequently undergoes charge transfer with a redox-active species in the electrolyte, which in turn reacts with a counter electrode, completing the circuit. To improve device performance, each component must be optimized. While research in n-type DSSCs has examined all of these components in depth,<sup>5,7–14</sup> prior studies on p-type DSSCs have prioritized the semiconductor and chromophore<sup>6,15–18</sup> or the identity of the redox couple in the electrolyte.<sup>19,20</sup> As a result, the energetics of common electrolytes may be poorly optimized for p-type DSSCs. Here, we examine the impact of spectator metal cations in the electrolytes and find it has a substantial impact on performance.

Although they are nominally spectators that do not participate in redox reactions, cation species are known to have significant impact in TiO<sub>2</sub> n-type DSSCs.<sup>7,8,13,21–25</sup> The cations adsorb to electrode surfaces,<sup>25</sup> altering the charge equilibrium at the semiconductor–electrolyte interface and causing a shift in the flat-band potential ( $V_{FB}$ ) of the semiconductor.<sup>26</sup> Studies on mesoporous anatase TiO<sub>2</sub> have suggested that cations can intercalate into the lattice and that

the potential drop occurs across the semiconductor–solution interface rather than from band bending within the semiconductor.<sup>27</sup> Previous studies have indicated that cation identity could have effects on NiO-based DSSCs as well. The concentration of Li<sup>+</sup> in solution has been found to affect the position of the  $V_{FB}$  in NiO DSSCs as well as the performance of devices overall.<sup>28</sup> In addition, the identity of the cation in solution has been shown to affect the electrochemical behavior of devices, especially in the potential window wherein surface-based trap states are located.<sup>29–32</sup> These states are known to have considerable impact on the performance of NiO DSSCs and may be the primary source of recombination in devices.<sup>29,33,34</sup> They are often linked to oxidized Ni sites at defects in the lattice,<sup>32,35</sup> although some studies have also linked the apparent states to cation adsorption and desorption.<sup>29,30</sup> However, in all prior studies only monovalent cations were examined, and in this work the influence of higher valence metal cations is studied.

In an ideal case, the open-circuit voltage ( $V_{OC}$ ) of a DSSC is related to the potential difference between the Nernstian potential of the redox couple and the quasi-Fermi level of the semiconductor.<sup>26</sup> Therefore, the  $V_{OC}$  can in principle be

**Received:** October 3, 2019

**Accepted:** January 31, 2020

**Published:** January 31, 2020



increased by increasing that difference, either by changing the redox couple, changing the semiconductor, or shifting the  $V_{FB}$  of the semiconductor by altering the surface electrostatics through the surface charge equilibrium. Altering the cation in solution offers a potentially straightforward method for altering surface charge and effective surface dipoles, thereby controlling the device  $V_{OC}$ . Charge injection efficiencies and device photocurrent have also been found to be dependent upon the surface electrostatics, with charge injection yields and photocurrent in  $TiO_2$  films tending to increase as the  $V_{OC}$  decreases for electrochemically positive potential shifts of the  $TiO_2$  band edge.<sup>8,13,25</sup>

One of the most common electrolyte systems in both p- and n-type DSSCs utilizes the  $I^-/I_3^-$  redox couple in acetonitrile,<sup>36</sup> which has been extensively used for devices with both  $NiO$ <sup>17</sup> and  $TiO_2$ .<sup>2,36</sup> An alternative electrolyte, which tends to produce higher  $V_{OC}$  values with  $NiO$ , uses the redox couple tris(4,4'-di-*tert*-butyl-2,2'-dipyridyl)cobalt(II/III) perchlorate (denoted  $Co^{II/III}$ ) in propylene carbonate.<sup>19,20</sup> Here, we compare the effects of  $Li^+$ ,  $Mg^{2+}$ , and  $Al^{3+}$  on the performance of  $NiO$  DSSCs using both the  $I^-/I_3^-$  and the  $Co^{II/III}$  electrolyte systems. In the  $Co^{II/III}$  system,  $Na^+$ ,  $Sr^{2+}$ , and  $Ca^{2+}$  were also examined to determine the effect of ionic radius and charge density. The two redox couples also allow us to compare the effect of cationic versus anionic species, which may have different interactions with cations adsorbed to the  $NiO$  surface. We fabricate  $NiO$  DSSCs<sup>29</sup> using the chromophore 4-(bis(4-(2,2-dicyanovinyl)thiophene-2-yl)phenylamino)benzoic acid, denoted **P1**,<sup>17</sup> and we use electrochemical impedance spectroscopy (EIS) to understand the origins of the shift in device metrics.

## 2. EXPERIMENTAL SECTION

**Materials and Reagents.** Acetonitrile (99.6%), iodine (>99.99%), lithium perchlorate (>95.0%), calcium perchlorate tetrahydrate (99%), magnesium iodide (98%), magnesium perchlorate (ACS reagent grade), aluminum iodide (>95%), aluminum perchlorate nonahydrate (98%),  $\alpha$ -terpineol (anhydrous), and ethyl cellulose (300 cP viscosity) were all purchased from Sigma-Aldrich. Strontium perchlorate trihydrate (98%) and anhydrous sodium perchlorate (>98%) were purchased from Alfa Aesar. Hydrated salts were dried under vacuum before use. Absolute ethanol was purchased from Fisher Scientific.  $NiO$  nanoparticles (product #28N-0801) were purchased from Inframat Advanced Materials. 1,3-Dimethylimidazolium iodide and 25  $\mu m$  thick Surlyn polymer were purchased from Solaronix. **P1** chromophore was purchased from Dyenamo. All chemicals were used as received. Fluorine-doped tin oxide (FTO) glass (TEC 15  $\Omega \cdot cm^2$ ) was purchased from Hartford glass and cleaned with typical organic solvents and sonication. Tris(4,4'-di-*tert*-butyl-2,2'-dipyridyl)cobalt (II/III) perchlorate, denoted  $Co^{II/III}$ , was synthesized according to previously published methods.<sup>37</sup>

**Electrolyte Preparation.** Iodide electrolytes were prepared by dissolving solid  $I_2$  in acetonitrile to produce a 5 mM solution. An iodide salt ( $LiI$ ,  $MgI_2$ , or  $AlI_3$ ) was then added to yield a solution that is 5 mM in iodine and 1.0 M in the salt. Because of the highly exothermic enthalpy of solvation for  $AlI_3$  in acetonitrile (and vigorous reaction with water), addition was performed slowly with glassware placed in an ice bath.  $Co^{II/III}$  solutions were prepared by dissolving equal moles of tris(4,4'-di-*tert*-butyl-2,2'-dipyridyl)cobalt(II) perchlorate and tris(4,4'-di-*tert*-butyl-2,2'-dipyridyl)cobalt(III) perchlorate in propylene carbonate to produce a solution 0.1 M in both  $Co^{II}$  and  $Co^{III}$ . The perchlorate salt of interest was then added to produce a 0.1 M solution. Note that the perchlorate salt solutions would degrade the electrolyte over time, so solutions were prepared on the same day as

testing. Perchlorate salts are powerful oxidizers and have been known to be explosive, so they should be handled with care.

**$NiO$  Electrode Preparation and Solar Cell Fabrication.**  $NiO$  spin-coating paste was prepared by using a literature method with Inframat  $NiO$  nanoparticles and standard homogenization techniques.<sup>38</sup>  $NiO$  paste was applied to FTO glass via spin-coating. Films were then annealed in a humidity-controlled furnace (<20% humidity) at 450  $^\circ C$  for 40 min. Annealed films were submerged in a 0.3 mM solution of **P1** dye for 1 h. Platinum counter electrodes were fabricated by drop-casting 5 mM chloroplatinic acid solution in isopropanol on FTO glass with a sandblasted hole. The alcohol was allowed to evaporate, and then films were annealed at 380  $^\circ C$  for 30 min. DSSCs were sandwiched with 25  $\mu m$  thick Surlyn polymer gasket by using a heating apparatus. Sandwiched devices were vacuum-backfilled with electrolyte and then sealed with Surlyn and microscope coverslip.

**Solar Cell Characterization.** Devices were illuminated by using a Newport Oriel 94021A solar simulator with AM 1.5G filter and calibrated to 1 sun with a certified reference Newport 91150 V solar cell. Electrical measurement were performed with a Keithley 2636A sourcemeter. Four cells were tested for each electrolyte examined.

**Electrochemical Analysis.**  $NiO$  electrodes were prepared as previously stated. Exposed FTO was masked with Kapton tape. Mott–Schottky tests were performed in a three-electrode setup in bulk solution using a CH Instruments 604 E potentiostat at 100 Hz utilizing a Ag/AgCl reference electrode,  $NiO$  working electrode, 0.1 M perchlorate salt electrolyte, and Pt mesh counter. No redox mediator was present in the solution for Mott–Schottky analysis. EIS was performed by using a Gamry PCI4-G750-51087 potentiostat in a two-electrode setup on assembled DSSC devices under 1 sun illumination in the frequency range  $10^{-1}$ – $10^5$  Hz. All EIS devices contained dye-loaded  $NiO$ . Devices were illuminated by using a Newport Oriel 91191-1000 solar simulator calibrated with a AM 1.5G filter calibrated to 1 sun illumination.

## 3. RESULTS

**Shifts in  $V_{fb}$  with Cation.** Figure 1 displays the change in  $V_{fb}$  measured by Mott–Schottky analysis with various cations by using the Mott–Schottky equation

$$C^{-2} = \frac{2}{\epsilon \epsilon_0 A^2 e N_A} \left( V - V_{fb} - \frac{k_B T}{e} \right) \quad (1)$$

where  $C$  is capacitance,  $V$  is applied potential,  $A$  is the area of the electrode,  $N_A$  is the effective density of dopant acceptors,  $k_B$  is the Boltzmann constant,  $T$  is temperature,  $e$  is fundamental charge,  $\epsilon$  is the relative static dielectric constant of the semiconductor, and  $\epsilon_0$  is the dielectric constant of free space. Figures 1A and B plot  $C^{-2}$  as a function of  $V$  for a measurement at 100 Hz (see Figure S1 for unnormalized plots and data at other frequencies), where the  $x$ -intercept from fits to the linear regime are used to determine an effective  $V_{fb}$  and to evaluate trends in  $V_{fb}$  with cation, as summarized in Tables 1 and 2.<sup>39</sup> The data in acetonitrile (Table 1) show substantial changes in the measured  $V_{fb}$  as the cation is varied, progressively shifting to more positive electrochemical potentials as  $Na^+ < Li^+ < Sr^{2+} < Ca^{2+} < Mg^{2+} < Al^{3+}$  (Figure 1C), consistent with reports on  $TiO_2$  cation effects.<sup>8,7,14,22</sup> Even for cations with the same valence charge, differences in  $V_{fb}$  are observed, with a relatively small 0.05 V difference between  $Na^+$  and  $Li^+$  and a substantial 0.37 V difference between  $Sr^{2+}$  and  $Mg^{2+}$ . Moreover,  $Al^{3+}$  produces a shift 0.51 V more positive than  $Mg^{2+}$  and 1.01 V more positive than  $Na^+$ . Data in propylene carbonate (Table 2 and Figure 1B) show that solvent also affects the  $V_{fb}$ , although the trends in propylene carbonate are generally the same as acetonitrile. However, unlike in acetonitrile,  $Sr^{2+}$  and  $Ca^{2+}$  show  $V_{fb}$  slightly

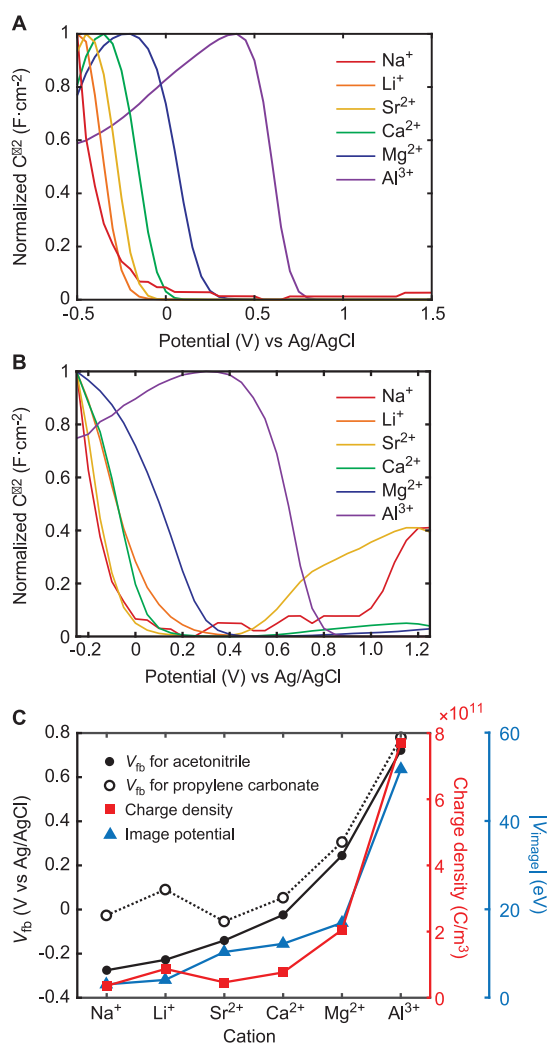


**Figure 1.** Shifts in  $V_{fb}$  with cation. Normalized Mott–Schottky plots at 100 Hz for mesoporous NiO film working electrodes and Pt mesh counter with a 0.1 M  $X(ClO_4)_m$  and no redox mediator in (A) acetonitrile or (B) propylene carbonate electrolyte with  $X = Na^+$  (red),  $Li^+$  (orange),  $Sr^{2+}$  (yellow),  $Ca^{2+}$  (green),  $Mg^{2+}$  (blue), and  $Al^{3+}$  (purple), where  $n$  equals the cation charge. (C)  $V_{fb}$  (open and closed black circles; left-hand axis), charge density (red squares; first right-hand axis), and  $|V_{image}|$  (blue triangles; second right-hand axis) as a function of cation in acetonitrile (closed black circles) and propylene carbonate (open black circles). All cations were introduced as perchlorate salts in 0.1 M concentration.

**Table 1.**  $V_{fb}$  of Mesoporous NiO Electrodes in Acetonitrile with 0.1 M  $X(ClO_4)_m$  ( $X = Na^+$ ,  $Li^+$ ,  $Sr^{2+}$ ,  $Ca^{2+}$ ,  $Mg^{2+}$ , and  $Al^{3+}$ ) Measured at 100 Hz

cation	$Na^+$	$Li^+$	$Sr^{2+}$	$Ca^{2+}$	$Mg^{2+}$	$Al^{3+}$
$V_{fb}$ (V vs Ag/AgCl)	-0.292	-0.247	-0.162	-0.028	0.210	0.720

**Table 2.**  $V_{fb}$  of Mesoporous NiO Electrodes in Propylene Carbonate with 0.1 M  $X(ClO_4)_m$  ( $X = Na^+$ ,  $Li^+$ ,  $Sr^{2+}$ ,  $Ca^{2+}$ ,  $Mg^{2+}$ , and  $Al^{3+}$ ) Measured at 100 Hz

cation	$Na^+$	$Li^+$	$Sr^{2+}$	$Ca^{2+}$	$Mg^{2+}$	$Al^{3+}$
$V_{fb}$ (V vs Ag/AgCl)	-0.028	0.089	-0.055	0.052	0.305	0.779

more negative than  $Li^+$ , and  $Sr^{2+}$  is also slightly negative of  $Na^+$ . Charge density, based on the effective ionic radius,<sup>40</sup> and image charge potential,  $|V_{image}|$ , are also plotted in Figure 1C for each cation to determine how well the shifts in  $V_{fb}$  correlate with these values, as discussed below and in section 4.

**DSSC Devices.** Mesoporous NiO films were fabricated into DSSC devices with the P1 chromophore by using multiple distinct electrolyte solutions, varying both the cation and redox couple. Current density–voltage ( $J$ – $V$ ) characterization was performed for all devices in the dark and under simulated AM1.5G 1 sun illumination, with all photovoltaic metrics, including  $V_{OC}$ , short-circuit current density ( $J_{SC}$ ), fill factor (FF), power-conversion efficiency ( $\eta$ ), dark saturation current density ( $J_0$ ), and ideality factor ( $n$ ), tabulated in Table 3. Representative  $J$ – $V$  curves for the  $I^-/I_3^-$  electrolyte in acetonitrile, created by using 1.0 M  $LiI$  and 1.0 M  $MgI_2$  with 5 mM  $I_2$ , as typical for this electrolyte, are shown in Figure 2A. When  $Li^+$  is exchanged for  $Mg^{2+}$  at a 1.0 M concentration, the  $V_{OC}$  increases by  $\sim 62\%$  while  $J_{SC}$  remains the same within error. Devices with  $Al^{3+}$  at 1.0 M were found to yield negligible photocurrent (Figure S2) most likely because of nearly complete desorption of dye from the NiO surface (Figure S3). However, the low current may also be partially attributable to the substantial shift of the valence band edge, which may preclude efficient charge injection from the chromophore due to misalignment of the valence band edge with the chromophore’s excited-state oxidative potential.<sup>41</sup> Figure 2B displays representative  $J$ – $V$  curves for the  $Co^{II/III}$  redox couple with  $Li^+$ ,  $Mg^{2+}$ , and  $Al^{3+}$  at a concentration of 0.1 M, which was chosen for consistency with prior studies in this electrolyte.<sup>19</sup> For  $Li^+$ ,  $V_{OC}$  is  $\sim 97$  mV higher than the  $I^-/I_3^-$  system, which is primarily due to the change in the redox potential and differing kinetics of recombination and regeneration of the redox couple in solution.<sup>19,36,41</sup> Substitution of  $Mg^{2+}$  for  $Li^+$  with  $Co^{II/III}$  increases  $V_{OC}$  by 55%, yielding a champion device in this system with a  $V_{OC}$  of 338 mV. Although the  $Al^{3+}$  devices again exhibited low  $J_{SC}$  most likely for the same reasons as observed for  $I^-/I_3^-$ , a champion  $V_{OC}$  of 351 mV was nevertheless observed by using this chromophore.<sup>42</sup> The  $J_{SC}$  for  $Mg^{2+}$  was approximately unchanged compared to that for  $Li^+$ .

To probe the effect of cation charge density (plotted in Figure 1C),  $J$ – $V$  curves were collected for  $Na^+$  and  $Li^+$  (Figure 3A) and for  $Sr^{2+}$ ,  $Ca^{2+}$ , and  $Mg^{2+}$  (Figure 3B) with  $Co^{II/III}$  in propylene carbonate. For each cation charge,  $V_{OC}$  exhibits a minor but reproducible increase with increasing charge density, as exemplified by the champion devices for each cation and electrolyte combination shown in Figures 3A and 3B. The data show that the effect of ionic radius is small relative to the effect of cation charge. For instance,  $Na^+$  and  $Ca^{2+}$  have similar ionic radii, yet  $Ca^{2+}$  has a charge density nearly 2-fold higher and an average  $V_{OC} \sim 106$  mV higher than  $Na^+$ , demonstrating that charge density is a key quantity to understand the changes in  $V_{OC}$ .

The dark  $J$ – $V$  curves (dashed lines in Figures 2 and 3) were fit to the ideal diode equation

$$J = J_0 \left( \exp \left( \frac{qV}{nk_B T} \right) - 1 \right) \quad (2)$$

to extract the dark saturation current density  $J_0$  and the ideality factor  $n$ , where  $n$  is related to the recombination parameter  $\beta$

Table 3. Summary of DSSC Performance

cation/redox couple <sup>a</sup>	cation conc (M)	$J_{SC}$ (mA/cm <sup>2</sup> )	$V_{OC}$ (mV)	FF (%)	$\eta$ (%)	$J_0$ ( $\mu$ A/cm <sup>2</sup> )	$n$
Li <sup>+</sup> /I	1.0	1.07 ± 0.26	106 ± 9	31.4 ± 0.8	0.036 ± 0.010	14.7 ± 8.0	1.40 ± 0.08
Mg <sup>2+</sup> /I	1.0	0.92 ± 0.15	172 ± 3	36.0 ± 0.8	0.057 ± 0.008	3.26 ± 0.6	1.57 ± 0.04
Al <sup>3+</sup> /I	1.0	0.013 ± 0.007	2.61 ± 1.50	20.6 ± 4.0	(9.78 ± 9.66) × 10 <sup>-6</sup>	(5.58 ± 2.67) × 10 <sup>-5</sup>	3.91 ± 1.70
Na <sup>+</sup> /Co	0.1	0.77 ± 0.04	192 ± 10	28.0 ± 0.3	0.042 ± 0.004	54.2 ± 4.5	4.37 ± 0.12
Li <sup>+</sup> /Co	0.1	0.76 ± 0.02	203 ± 16	28.1 ± 0.3	0.043 ± 0.002	47.8 ± 9.7	4.26 ± 0.31
Sr <sup>2+</sup> /Co	0.1	0.84 ± 0.11	286 ± 7	27.6 ± 2.3	0.066 ± 0.006	23.8 ± 7.9	4.29 ± 0.63
Ca <sup>2+</sup> /Co	0.1	0.57 ± 0.11	303 ± 11	30.4 ± 6.0	0.052 ± 0.014	17.1 ± 7.5	4.35 ± 0.84
Mg <sup>2+</sup> /Co	0.1	0.72 ± 0.27	315 ± 18	36.4 ± 6.7	0.078 ± 0.026	9.4 ± 3.9	3.15 ± 0.34
Al <sup>3+</sup> /Co	0.1	0.04 ± 0.01	314 ± 26	44.8 ± 2.8	0.005 ± 0.003	1.4 ± 0.3	4.91 ± 0.35

<sup>a</sup>The redox couple was either I<sup>-</sup>/I<sub>3</sub><sup>-</sup> (I) in acetonitrile or Co<sup>II/III</sup> (Co) in propylene carbonate.

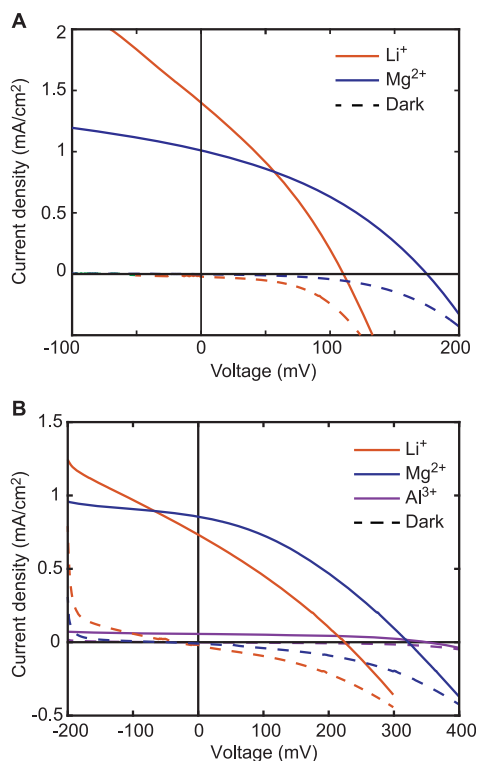


**Figure 2.** Effect of cation valence charge on DSSC devices. Champion  $J$ - $V$  curves in the dark (dashed lines) and under 1 sun illumination (solid lines) for DSSCs containing (A) 1.0 M Li<sup>+</sup> (orange) and 1.0 M Mg<sup>2+</sup> (blue) in I<sup>-</sup>/I<sub>3</sub><sup>-</sup> electrolyte with acetonitrile and (B) 0.1 M Li<sup>+</sup> (orange), 0.1 M Mg<sup>2+</sup> (blue), and 0.1 M Al<sup>3+</sup> (violet) in Co<sup>II/III</sup> electrolyte with propylene carbonate.

(discussed in section 4) as  $n = 1/\beta$ . Figure 3C summarizes the trends in  $V_{OC}$  and  $J_0$  across all the cations and redox couples examined, arranging ions from largest and least charged to smallest and most charged in their respective electrolytes. A clear trend in both  $V_{OC}$  and  $J_0$  is apparent, with  $V_{OC}$  increasing and  $J_0$  decreasing as cations become smaller and more positively charged. Similarly, the trend in  $J_{SC}$  as a function of cation is shown in Figure 3D and shows a slight tendency to decrease as  $V_{OC}$  increases.

**EIS Results.** The impact of the cation on interfacial charge transfer and recombination was examined by using EIS. Nyquist plots were constructed for each DSSC device (see Figures S4–S7), and representative plots for 0.1 M Li<sup>+</sup> in Co<sup>II/III</sup> electrolyte at various potentials under 1 sun illumination are displayed in Figure 4A. Two distinct semicircles are apparent, indicative of two charge-transfer

regimes. The size of these semicircles varies with applied bias, and the strong dependence of the larger semicircle on applied bias indicates it is likely linked to the semiconductor/electrolyte interface whereas the smaller semicircle with weaker dependence on bias is likely linked to the Pt counter electrode/electrolyte interface, in accord with prior studies on NiO.<sup>43,44</sup> The devices were thus modeled using an equivalent circuit consisting of a modified double Randles cell (inset of Figure 4A), incorporating a charge-transfer resistance ( $R_{CT,S}$ ) and capacitance ( $C_S$ ) for the semiconductor/electrolyte interface, a charge-transfer resistance ( $R_{CT,E}$ ) and capacitance ( $C_E$ ) for the counter electrode/electrolyte interface (Tables S1 and S2), and a series resistance ( $R_S$ ) for the semiconductor.<sup>43,44</sup> A constant phase element is used to model nonideal capacitors.<sup>43</sup> The impedance,  $Z$ , of such a component is expressed as  $[(i\omega)^\gamma Y_0]^{-1}$ , where  $i$  is the imaginary number,  $\omega$  is the ac frequency,  $\gamma$  is an empirical constant, and  $Y_0$  is an empirical admittance value with dimension  $S \cdot s^\gamma$ . Capacitance values,  $C$ , for constant phase elements were then calculated as  $(Y_0 R)^{1/\gamma} / R$ , where  $R$  is the associated parallel resistance, and Tables S3 and S4 tabulate values used for capacitance calculations. Tables 4 and 5 summarize all extracted EIS parameters for the I<sup>-</sup>/I<sub>3</sub><sup>-</sup> and Co<sup>II/III</sup> electrolyte systems, respectively, where time constants  $\tau_s$  and  $\tau_e$  for the semiconductor and electrolyte were calculated as  $R_{CT,S}C_S$  and  $R_{CT,E}C_E$ , respectively. These parameters were measured for devices with 0 V applied bias and at  $V_{OC}$  to examine how cations affect the potential-dependent response of the devices.

#### 4. DISCUSSION

**Shifts in  $V_{fb}$  with Cation.** Upon comparison of the changes in  $V_{fb}$  and charge density in Figure 1C, the relative shifts in both quantities qualitatively follow the same trend, consistent with prior reports in TiO<sub>2</sub> and NiO that observed the shift in conduction band edge position to increase with increasing cation charge density or concentration.<sup>21,22,24,30</sup> If we assume all cations adsorb to the NiO surface with the same surface density ( $\rho$ ; units of cm<sup>-2</sup>) and generate an effective surface dipole ( $\mu$ ; units of C·cm) proportional to the charge and ionic radius of the cation, the shift in  $V_{fb}$  from the array of surface dipoles can be approximated as  $\mu\rho/2\epsilon_0$ . However, for each charge, this expression would predict a decreasing shift in  $V_{fb}$  with increasing charge density (i.e., smaller ionic radius) assuming constant  $\rho$ ; however, the opposite trend (increasing shift with increasing charge density) is observed. This theory suggests that  $\rho$  may also vary with cation and increases with increasing charge density. To understand a potential origin of this trend, we consider a simple model in which the cation is assumed to produce an image charge at the NiO surface.<sup>45</sup> The

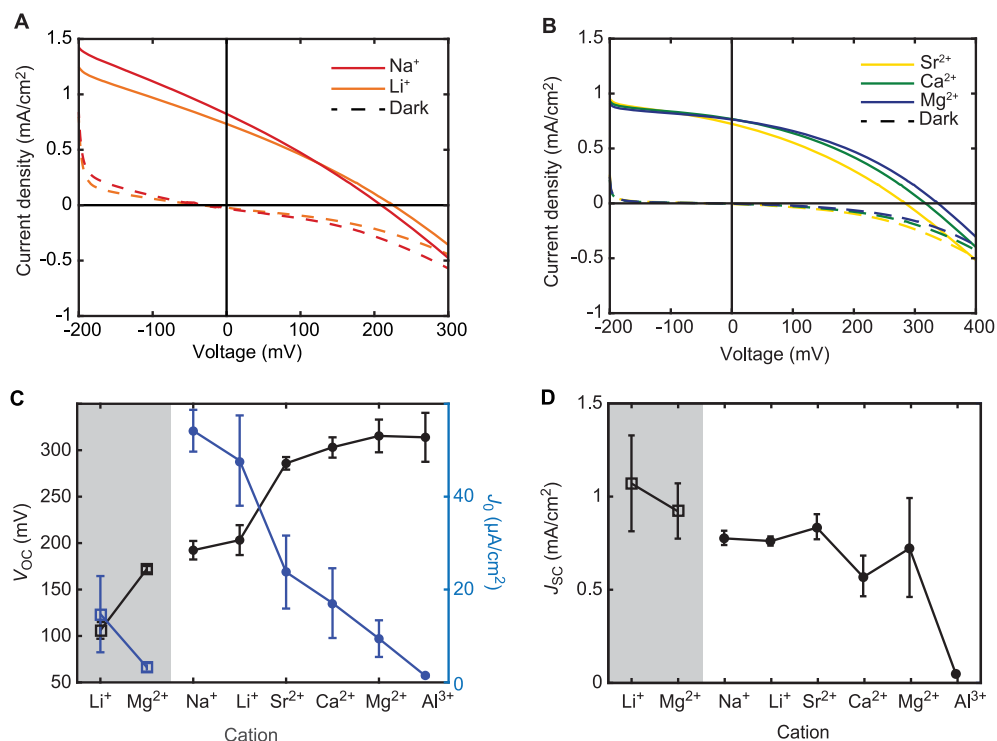


**Figure 3.** Effect of cation charge density on DSSC devices. (A, B)  $J$ - $V$  curves for Co<sup>II/III</sup>-based DSSCs with 0.1 M Na<sup>+</sup> or Li<sup>+</sup> singly charged cations (panel A) and 0.1 M Sr<sup>2+</sup>, Ca<sup>2+</sup>, and Mg<sup>2+</sup> doubly charged cations (panel B). Data for Li<sup>+</sup> and Mg<sup>2+</sup> are reproduced from Figure 2 for clarity. (C)  $V_{OC}$  (left-hand axis and black marker symbols) and  $J_0$  (right-hand axis and blue marker symbols) for various cations with the  $\Gamma^-/I_3^-$  electrolyte (squares and shaded region) and Co<sup>II/III</sup> electrolyte (circles). (D)  $J_{SC}$  for various cations with the  $\Gamma^-/I_3^-$  electrolyte (squares and shaded region) and Co<sup>II/III</sup> electrolyte (circles).

image potential,  $V_{image}$ , at a dielectric surface can be calculated as

$$V_{image} = -\frac{m^2 e^2 \delta}{16\pi\epsilon_0 z} \quad (3)$$

where  $m$  is the cation valence charge,  $z$  is the distance of the charge to the NiO surface,  $\delta$  is  $(\epsilon_s - 1)/(\epsilon_s + 1)$ , and  $\epsilon_s$  is the static dielectric constant of NiO ( $\epsilon_s = 12$ ).<sup>45</sup> Figure 1C also plots the magnitude of  $V_{image}$  if the cation is treated as a point charge located one ionic radius<sup>40</sup> ( $R_i$ ) from the semiconductor surface, i.e.,  $z = R_i$ . The trend in magnitude of  $V_{image}$  with cation follows the trend of  $V_{fb}$  relatively well for all cations in acetonitrile and propylene carbonate, although it does not explain the difference between monovalent and divalent cations in the latter. Generally, however, the overall agreement in trends suggests that cations with higher  $|V_{image}|$  exhibit proportionally higher  $\rho$  due to greater attraction to the NiO surface, resulting in the larger measured shifts of  $V_{fb}$ . However, effects from the solvent and chemisorbed chromophore likely play an important role in the final determination of the effective surface dipoles and  $V_{fb}$  in the operational devices. Image potential provides only a qualitative estimate of the relative energetics associated with different cations and is not intended to be a rigorous description of the electrostatic potential of the NiO surface in electrolyte solution.

**EIS Analysis.** Figures 4B and 4C depict values of  $R_{CT,S}$ ,  $C_S$ , and  $\tau_S$  as a function of applied bias under 1 sun illumination for the Co<sup>II/III</sup> electrolyte by using the Li<sup>+</sup> and Mg<sup>2+</sup> cations, respectively. In general,  $R_{CT,S}$  decreases in all systems, including  $\Gamma^-/I_3^-$ , as bias is increased, but  $C_S$  tends to increase. For  $R_{CT,S}$ , the increased accumulation of charge as the applied

voltage,  $V$ , approaches  $V_{OC}$  causes increased recombination and thereby lowers  $R_{CT,S}$ . This change in recombination resistance can be nominally expressed as

$$R_{CT,S} = R_0 \exp\left(\frac{-e\beta V}{k_B T}\right) \quad (4)$$

where  $R_0$  is the value of  $R_{CT,S}$  at short circuit.<sup>46</sup> Similarly, because of the increased rate of change of charge accumulation, the values of  $C_S$  are expected to exponentially increase with higher applied voltage as

$$C_S = C_0 \exp\left(\frac{e\beta V}{k_B T}\right) \quad (5)$$

where  $C_0$  is the value of  $C_S$  at short circuit. Nominally, for an ideal system with linear recombination terms ( $\beta = 1$ ) and no trapping of charge carriers in localized states,<sup>47</sup> the value of  $\tau_S = R_{CT,S}C_S$  does not change with  $V$ ; however, the data generally show a decrease of  $\tau_S$  with applied potential (e.g., Figure 4B), in accord with prior studies on NiO,<sup>43</sup> whereas data for divalent cations in Co<sup>II/III</sup> show a slight increase. Note that  $C_S$  and  $R_{CT,S}$  for divalent cations with Co<sup>II/III</sup> (Figure 4C) appear to show two regimes: one below and one above 150–200 mV, with two different slopes. These two regimes could suggest a difference in the states being accessed in these potential windows (e.g., bulk/surface traps vs band edge states), although future investigation will be needed.

Changes in  $\tau_S$  can be attributed to nonidealities of NiO that cause nonlinear recombination ( $\beta < 1$ ) and to the trapping of charge carriers in localized states.<sup>46</sup> In the case of nonlinear recombination,  $\tau_S = (k_{rec}p^{\beta-1})^{-1}$ , with  $k_{rec}$  the rate constant

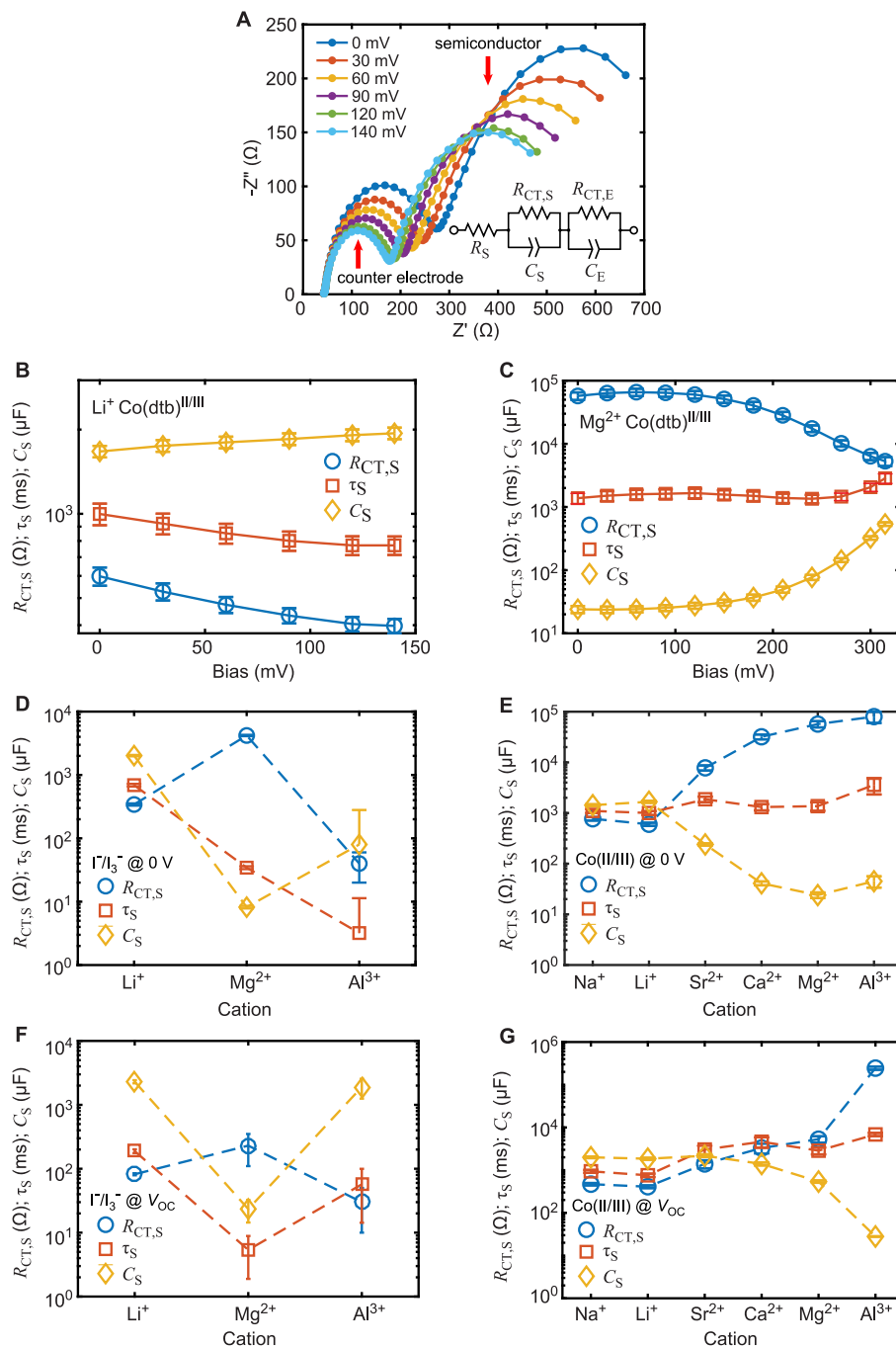


**Figure 4.** EIS analysis of cation effects. (A) Representative Nyquist plot for a DSSC at various applied biases with the 0.1 M  $\text{Li}^+$  in  $\text{Co}^{\text{II/III}}$  electrolyte. Bias was increased from 0 mV to  $\sim V_{\text{OC}}$  for the device under 1 sun illumination. Inset: equivalent circuit used for EIS analysis. (B)  $R_{\text{CT,S}}$ ,  $C_S$ , and  $\tau_S$  as a function of applied bias for 0.1 M  $\text{Li}^+$  in  $\text{Co}^{\text{II/III}}$  electrolyte, as determined from fitting the data in panel A. (C)  $R_{\text{CT,S}}$ ,  $C_S$ , and  $\tau_S$  as a function of applied bias for 0.1 M  $\text{Mg}^{2+}$  in  $\text{Co}^{\text{II/III}}$  electrolyte. (D–G)  $R_{\text{CT,S}}$ ,  $C_S$ , and  $\tau_S$  as a function of cation at short circuit (panels D and E) and open circuit (panels F and G) for the iodide (panels D and F) and  $\text{Co}^{\text{II/III}}$  (panels E and G) electrolytes.

**Table 4.** EIS Parameters for Electrolytes 1.0 M in Cation Concentration with the  $\text{I}^-/\text{I}_3^-$  Redox Couple in Acetonitrile under 1 sun Illumination

cation	voltage	$R_{\text{CT,S}}$ ( $\Omega$ )	$C_S$ ( $\mu\text{F}$ )	$\tau_S$ (ms)	$R_S$ ( $\Omega$ )
$\text{Li}^+$	0 V	$342 \pm 14$	$2020 \pm 50$	$690 \pm 30$	$33 \pm 2$
$\text{Mg}^{2+}$	0 V	$4200 \pm 100$	$8.2 \pm 0.4$	$34 \pm 2$	$29.0 \pm 0.3$
$\text{Al}^{3+}$	0 V	$40 \pm 20$	$80 \pm 200$	$3 \pm 8$	$56.5 \pm 1.3$
$\text{Li}^+$	$V_{\text{OC}}$	$82 \pm 3$	$2300 \pm 130$	$190 \pm 10$	$41 \pm 3$
$\text{Mg}^{2+}$	$V_{\text{OC}}$	$230 \pm 120$	$23 \pm 9$	$5.4 \pm 3.5$	$30.9 \pm 0.4$
$\text{Al}^{3+}$	$V_{\text{OC}}$	$30 \pm 20$	$1900 \pm 650$	$60 \pm 40$	$56.8 \pm 1.3$

**Table 5.** EIS Parameters for Electrolytes 0.1 M in Cation Concentration with the Co<sup>II/III</sup> Redox Couple in Propylene Carbonate under 1 sun Illumination

cation	voltage	$R_{CT,S}$ ( $\Omega$ )	$C_S$ ( $\mu F$ )	$\tau_S$ (ms)	$R_S$
Na <sup>+</sup>	0 V	770 ± 60	1430 ± 60	1100 ± 100	49.8 ± 0.4
Li <sup>+</sup>	0 V	600 ± 44	1670 ± 80	1000 ± 90	43.4 ± 0.4
Sr <sup>2+</sup>	0 V	7800 ± 900	240 ± 12	1870 ± 240	48.6 ± 0.4
Ca <sup>2+</sup>	0 V	32000 ± 3500	41 ± 4	1310 ± 180	54.6 ± 0.4
Mg <sup>2+</sup>	0 V	57000 ± 8000	24 ± 3	1370 ± 260	58.4 ± 0.4
Al <sup>3+</sup>	0 V	80000 ± 20000	45 ± 11	3600 ± 1300	58.5 ± 0.5
Na <sup>+</sup>	$V_{OC}$	470 ± 30	2000 ± 90	940 ± 70	47.5 ± 0.4
Li <sup>+</sup>	$V_{OC}$	410 ± 30	1850 ± 100	760 ± 70	82.7 ± 0.6
Sr <sup>2+</sup>	$V_{OC}$	1400 ± 300	2200 ± 150	3040 ± 680	49.9 ± 0.4
Ca <sup>2+</sup>	$V_{OC}$	3300 ± 850	1400 ± 100	4600 ± 1200	53.7 ± 0.4
Mg <sup>2+</sup>	$V_{OC}$	5300 ± 900	540 ± 30	2900 ± 500	50.2 ± 0.5
Al <sup>3+</sup>	$V_{OC}$	245000 ± 21000	30 ± 1	6900 ± 600	58.1 ± 1.2

for recombination in the  $\beta$ -recombination model and  $p$  the concentration of holes. In the case of charge-carrier trapping, a distribution of trap states above the band edge, which is common for disordered metal oxides such as NiO, can localize charge carriers and affect the carrier lifetime because of a potential-dependent trapping lifetime. Nonlinear recombination tends to increase lifetime with  $V$  (due to increase in  $p$ ) whereas trapping tends to decrease the lifetime. Thus, the decrease in  $\tau_S$  with increasing  $V$  with the Li<sup>+</sup> cation suggests a strong effect from charge-carrier trapping, consistent with reports on TiO<sub>2</sub> devices.<sup>22,24</sup> Although  $\tau_S$  decreases with bias for all monovalent ions, when divalent cations are used with the Co<sup>II/III</sup> redox couple in propylene carbonate,  $\tau_S$  increases slightly with bias. For instance,  $\tau_S$  increases from ~1370 to ~2900 ms going from short circuit to open circuit in Mg<sup>2+</sup>. This atypical behavior for DSSCs suggests a potentially favorable interaction between the cations at the NiO surface and the redox couple, which may act to reduce the effect of trap states on the observed lifetime. However, this favorable interaction does not exist for the I<sup>-</sup>/I<sub>3</sub><sup>-</sup> redox couple with Mg<sup>2+</sup>, which shows a decrease in lifetime with applied voltage, similar to the results with Li<sup>+</sup>.

As the cation is changed,  $R_{CT,S}$  and  $C_S$  change as a result of the shift in  $V_{fb}$ , analogous to the changes that occur as a result of the applied potential. As shown in the plots at short circuit (Figure 4D,E) and open circuit (Figure 4F,G) under 1 sun conditions for both electrolyte systems,  $R_{CT,S}$  tends to increase and  $C_S$  tends to decrease for increasingly positive shifts of  $V_{fb}$  (neglecting data for Al<sup>3+</sup>, which due to the desorption of chromophores from the interface has anomalous performance). The increase in  $R_{CT,S}$  likely originates from the decrease in charge accumulation at the semiconductor–solution interface, which reduces recombination. This change can be understood by considering how  $R_0$  and  $J_0$  depend on the valence band edge position ( $E_v$ ).<sup>47</sup>  $J_0$  can be expressed as

$$J_0 = eLk_{rec}p^\beta = eLk_{rec}N_v^\beta \exp(\beta(E_v - E_{redox})/k_B T) \quad (6)$$

where  $L$  is the thickness of the film,  $N_v$  is valence band effective density of states,  $E_v$  is the valence band edge position, and  $E_{redox}$  is the Nernstian potential of the redox couple.  $R_0$  can be related to  $J_0$  as

$$R_0 = \frac{k_B T}{eA\beta J_0} = \frac{k_B T}{e^2\beta ALk_{rec}N_v^\beta} \exp(-\beta(E_v - E_{redox})/k_B T) \quad (7)$$

where  $A$  is the projected area of the film and the expression for  $J_0$  from eq 5 has been substituted in on the right-hand side of eq 6. This expression predicts an exponential increase in  $R_0$  as the band edge shifts to increasingly positive electrochemical potentials (corresponding to more negative  $E_v$ ). The decrease in  $C_S$  with increasing shift in  $V_{fb}$  can similarly be understood by the decrease in the rate of change of charge density at the interface between the semiconductor and liquid. Using eq 6 and the relationships  $\tau_S = (k_{rec}p^{\beta-1})^{-1}$  and  $\tau_S = R_0C_0$ , we can express  $C_0$  as

$$C_0 = \frac{e^2 AL p}{k_B T} = \frac{e^2 AL N_v}{k_B T} \exp((E_v - E_{redox})/k_B T) \quad (8)$$

Equation 7 indicates that  $C_0$  should decrease exponentially with increasing shifts of the band edge position, which is qualitatively consistent with the changes of  $C_S$  with cation in Figure 4D–G.

Although  $\tau_S$  and thereby  $k_{rec}$  would in an ideal system be independent of  $E_v$ , the nonlinear recombination ( $\beta < 1$ ), trapping of charge carriers, and interactions of the surface, cation, and electrolyte cause the values to vary significantly. Switching from monovalent to divalent cations,  $\tau_S$  values are observed to remain approximately constant or slightly increase in the Co<sup>II/III</sup> devices but decrease by an order of magnitude or more with the I<sup>-</sup>/I<sub>3</sub><sup>-</sup> devices. The increase in  $\tau_S$  for Co<sup>II/III</sup> can potentially be attributed to a longer lifetime for the charge carriers trapped in localized states because the shift of the band edge increases the effective activation energy for detrapping. However, the increase may also be caused in part from a decrease in  $k_{rec}$  due to a favorable interaction between the cation and Co<sup>II/III</sup> redox couple, as also suggested by the potential-dependent data.

The decrease in  $\tau_S$  for I<sup>-</sup>/I<sub>3</sub><sup>-</sup> is somewhat surprising because the effects of carrier density  $p$  and trapping dynamics would be expected to be similar for Co<sup>II/III</sup> and I<sup>-</sup>/I<sub>3</sub><sup>-</sup> given the same NiO electrode. Instead, we hypothesize that the decrease is likely attributable to an unfavorable interaction between the cation and redox couple, which might, for instance, favor anion adsorption to or association with the NiO surface to increase recombination rates. This effect would manifest as an increase in  $k_{rec}$  thereby explaining the decrease in  $\tau_S$ . The increase in  $k_{rec}$  would also cause the magnitude of the increase in  $R_{CT,S}$  (and  $R_0$  at short circuit) to be smaller than would otherwise be expected. For comparison,  $R_0$  between Li<sup>+</sup> and Mg<sup>2+</sup> increases by a factor of ~95 for Co<sup>II/III</sup> but only by ~12 for I<sup>-</sup>/I<sub>3</sub><sup>-</sup>. An unfavorable interaction with I<sup>-</sup>/I<sub>3</sub><sup>-</sup> would be consistent with

the apparent favorable interaction with  $\text{Co}^{\text{II/III}}$ , as a change from anionic to cationic redox couple might be expected to produce the opposite trends.

**DSSC Device Discussion.** As determined from the  $J$ - $V$  curves, a reduction in  $J_0$  and increase in  $V_{\text{OC}}$  (Figure 3C) are observed for cations with increasing valence charge, increasing charge density, and increasing magnitude of  $V_{\text{image}}$ . This trend can be explained by the observed shifts in  $V_{\text{fb}}$  and  $E_v$  with cation. If we assume the shift in  $E_v$ ,  $\Delta E_v$ , is equal in magnitude to the shift in  $V_{\text{fb}}$ , i.e.,  $\Delta E_v = E_v - E_v' = -e\Delta V_{\text{fb}}$ , where  $E_v'$  is the initial band edge position, the shift would according to eq 5 produce a decrease in  $J_0$  by the factor  $\exp(\beta\Delta E_v/k_B T)$ . Similarly, the  $V_{\text{OC}}$  should increase by the amount  $\Delta V_{\text{OC}} = -\beta\Delta E_v = e\beta\Delta V_{\text{fb}}$ . Taking data in  $\text{Li}^+$  as the benchmark, the shifts in  $V_{\text{fb}}$  relative to  $\text{Li}^+$  (Figure 1 and Tables 1 and 2) do generally predict the correct direction of the shift in  $J_0$  and  $V_{\text{OC}}$  relative to values in  $\text{Li}^+$ ; however, it does not correctly predict the magnitude of the change if all other parameters in eq 5 are constant. For instance, in  $\text{I}^-/\text{I}_3^-$ , the magnitude of  $\Delta V_{\text{fb}}$  between  $\text{Li}^+$  and  $\text{Mg}^{2+}$  (457 mV) would predict a decrease in  $J_0$  by  $\sim 10^5$  and increase in  $V_{\text{OC}}$  by 276 mV if  $\beta$  is assumed to be 0.6 (approximately the value of  $\beta = 1/n$  from Table 3), yet a decrease by a factor of  $\sim 5$  and increase of 66 mV, respectively, are observed. However, the EIS analysis suggests that there may be an unfavorable interaction between the  $\text{I}^-/\text{I}_3^-$  redox couple and divalent cations at the NiO interface that leads to an increase in  $k_{\text{rec}}$ . For a change in  $k_{\text{rec}}$  by a factor  $\alpha$ ,  $J_0$  changes by the same factor and  $V_{\text{OC}}$  changes by the amount  $-(k_B T/\beta e) \ln(\alpha)$ . EIS for  $\text{I}^-/\text{I}_3^-$  in acetonitrile (Table 4) indicates a decrease in  $\tau_s$  by a factor of  $\sim 20$  at short circuit ( $V = 0$  V). Thus, if we assume this change results entirely from an increase in  $k_{\text{rec}}$  ( $\alpha \approx 20$ ),  $V_{\text{OC}}$  would decrease by  $\sim 130$  mV. Combining the expected effects from the shift in  $V_{\text{fb}}$  and increase in  $k_{\text{rec}}$  we expect the increase in  $V_{\text{OC}}$  to be 140–150 mV, in better agreement with experiment. Thus, the data suggest that although  $V_{\text{OC}}$  with  $\text{I}^-/\text{I}_3^-$  appreciably increases using  $\text{Mg}^{2+}$  instead of  $\text{Li}^+$  because of a reduced absolute rate of recombination from decreased charge carrier accumulation at the interface, the magnitude of the change is reduced because of an unfavorable interaction that enhances the rate constant for recombination.

For the  $\text{Co}^{\text{II/III}}$  redox couple in propylene carbonate, the magnitude of  $\Delta V_{\text{fb}}$  between  $\text{Li}^+$  and  $\text{Mg}^{2+}$  (216 mV) would predict a decrease in  $J_0$  by  $\sim 10$  and increase in  $V_{\text{OC}}$  by  $\sim 58$  mV if  $\beta$  is assumed to be 0.27 (using  $n = 1/\beta = 3.7$ , the average of the values in Table 3). A decrease of  $J_0$  by a factor of  $\sim 5$  and increase of  $V_{\text{OC}}$  by 112 mV are observed experimentally, which are in reasonable approximate agreement with the predictions. EIS on these devices (Table 5) indicates a relatively minimal change in  $\tau_s$  at short circuit. Thus, even though they do not provide quantitative predictions, the experimentally observed changes in  $V_{\text{OC}}$  and  $J_0$  can be qualitatively explained by shifts in  $V_{\text{fb}}$  and changes in  $k_{\text{rec}}$  with the electrolyte cation. The changes in  $J_{\text{SC}}$  with cation (Figure 3D) are relatively minor and can be attributed to changes in the charge injection efficiency of the chromophore due to the shifting band edge position, similar to that observed with  $\text{TiO}_2$ .<sup>8,13</sup>

## 5. CONCLUSION

Spectator cations in electrolyte solutions have been demonstrated to have significant effects on the band edge position of NiO and the properties and performance of NiO p-type DSSC devices. Spectator cations induce an effective dipole at the

semiconductor/electrolyte interface, altering the flat-band position of the valence band and altering the effective carrier lifetime and charge-transfer kinetics at the interface. The behavior of NiO generally follows that same trends as observed with n-type  $\text{TiO}_2$ , although the shifts in performance with cation are as expected, opposite of those observed with  $\text{TiO}_2$  because of the p-type nature of NiO. Upon comparison of the results of anionic  $\text{I}^-/\text{I}_3^-$  and cationic  $\text{Co}^{\text{II/III}}$  redox couples, the data provide preliminary evidence of unfavorable and favorable interactions with divalent spectator cations that may produce increases and decreases, respectively, in the rate constants for charge carrier recombination and affect the trapping of carriers in localized states. Despite these differences, the data strongly suggest the replacement of  $\text{Li}^+$  with  $\text{Mg}^{2+}$  can lead to immediate improvements in DSSC device metrics for both electrolyte systems. Overall, the results highlight the complex interplay between the NiO surface, cation, and electrolyte solution, which can sometimes exhibit competing trends that dictate the ultimate performance of devices.

## ■ ASSOCIATED CONTENT

### Supporting Information

The Supporting Information is available free of charge at <https://pubs.acs.org/doi/10.1021/acsaem.9b01955>.

Figures S1–S7 (PDF)

## ■ AUTHOR INFORMATION

### Corresponding Author

James F. Cahoon – Department of Chemistry, University of North Carolina at Chapel Hill, Chapel Hill, North Carolina 27599-3290; [orcid.org/0000-0003-1780-215X](https://orcid.org/0000-0003-1780-215X); Email: [jfcahoon@unc.edu](mailto:jfcahoon@unc.edu)

### Authors

Shannon M. McCullough – Department of Chemistry, University of North Carolina at Chapel Hill, Chapel Hill, North Carolina 27599-3290

Jake M. Evans – Department of Chemistry, University of North Carolina at Chapel Hill, Chapel Hill, North Carolina 27599-3290; [orcid.org/0000-0002-8721-5316](https://orcid.org/0000-0002-8721-5316)

Taylor Moot – Department of Chemistry, University of North Carolina at Chapel Hill, Chapel Hill, North Carolina 27599-3290

Aaron D. Taggart – Department of Chemistry, University of North Carolina at Chapel Hill, Chapel Hill, North Carolina 27599-3290; [orcid.org/0000-0003-4096-1351](https://orcid.org/0000-0003-4096-1351)

Ludovic Troian-Gautier – Department of Chemistry, University of North Carolina at Chapel Hill, Chapel Hill, North Carolina 27599-3290; [orcid.org/0000-0002-7690-1361](https://orcid.org/0000-0002-7690-1361)

Complete contact information is available at: <https://pubs.acs.org/doi/10.1021/acsaem.9b01955>

### Author Contributions

<sup>‡</sup>S.M.M. and J.M.E. equally contributed to this work.

### Notes

The authors declare no competing financial interest.

## ■ ACKNOWLEDGMENTS

This work was primarily funded by the University of North Carolina Energy Frontier Research Center (EFRC), “Alliance for Molecular Photoelectrode Design” (AMPED), funded by

the U.S. Department of Energy, Office of Science, Office of Basic Energy Sciences, under Award DE-SC0001011. This work made use of instrumentation at the Chapel Hill Analytical and Nanofabrication Laboratory (CHANL), a member of the North Carolina Research Triangle Nanotechnology Network (RTNN), which is supported by the NSF (ECCS-1542015) as part of the National Nanotechnology Coordinated Infrastructure (NNCI). J.F.C. and J.M.E. acknowledge support from an individual Cottrell Scholar Award (23394).

## REFERENCES

- (1) O'Regan, B.; Grätzel, M. A Low-Cost, High-Efficiency Solar Cell Based on Dye-Sensitized Colloidal TiO<sub>2</sub> Films. *Nature* **1991**, *353*, 737.
- (2) Grätzel, M. Dye-Sensitized Solar Cells. *J. Photochem. Photobiol. C* **2003**, *4*, 145–153.
- (3) He, J.; Lindström, H.; Hagfeldt, A.; Lindquist, S.-E. Dye-Sensitized Nanostructured p-Type Nickel Oxide Film as a Photocathode for a Solar Cell. *J. Phys. Chem. B* **1999**, *103*, 8940–8943.
- (4) Bandara, J.; Weerasinghe, H. Solid-State Dye-Sensitized Solar Cell with P-Type NiO as a Hole Collector. *Sol. Energy Mater. Sol. Cells* **2005**, *85*, 385–390.
- (5) Crossland, E. J. W.; Noel, N.; Sivaram, V.; Leijtens, T.; Alexander-Webber, J. A.; Snaith, H. J. Mesoporous TiO<sub>2</sub> Single Crystals Delivering Enhanced Mobility and Optoelectronic Device Performance. *Nature* **2013**, *495*, 215.
- (6) Flynn, C. J.; Oh, E. E.; McCullough, S. M.; Call, R. W.; Donley, C. L.; Lopez, R.; Cahoon, J. F. Hierarchically-Structured NiO Nanoplatelets as Mesoscale p-Type Photocathodes for Dye-Sensitized Solar Cells. *J. Phys. Chem. C* **2014**, *118*, 14177–14184.
- (7) O'Donnell, R. M.; Sampaio, R. N.; Barr, T. J.; Meyer, G. J. Electric Fields and Charge Screening in Dye Sensitized Mesoporous Nanocrystalline TiO<sub>2</sub> Thin Films. *J. Phys. Chem. C* **2014**, *118*, 16976–16986.
- (8) Kelly, C. A.; Farzad, F.; Thompson, D. W.; Stipkala, J. M.; Meyer, G. J. Cation-Controlled Interfacial Charge Injection in Sensitized Nanocrystalline TiO<sub>2</sub>. *Langmuir* **1999**, *15*, 7047–7054.
- (9) Maitani, M. M.; Tsukushi, Y.; Hansen, N. D. J.; Sato, Y.; Mochizuki, D.; Suzuki, E.; Wada, Y. Low-Temperature Annealing of Mesoscopic TiO<sub>2</sub> Films by Interfacial Microwave Heating Applied to Efficiency Improvement of Dye-Sensitized Solar Cells. *Sol. Energy Mater. Sol. Cells* **2016**, *147*, 198–202.
- (10) Sigdel, S.; Dubey, A.; Elbohy, H.; Aboagye, A.; Galipeau, D.; Zhang, L.; Fong, H.; Qiao, Q. Dye-Sensitized Solar Cells Based on Spray-Coated Carbon Nanofiber/TiO<sub>2</sub> Nanoparticle Composite Counter Electrodes. *J. Mater. Chem. A* **2014**, *2*, 11448–11453.
- (11) Wang, H.; Liu, Y.; Li, M.; Huang, H.; Xu, H. M.; Hong, R. J.; Shen, H. Multifunctional TiO<sub>2</sub> Nanowires-Modified Nanoparticles Bilayer Film for 3D Dye-Sensitized Solar Cells. *Optoelectron. Adv. Mater., Rapid Commun.* **2010**, *4*, 1166–1169.
- (12) Dell'Orto, E.; Raimondo, L.; Sassella, A.; Abboto, A. Dye-Sensitized Solar Cells: Spectroscopic Evaluation of Dye Loading on TiO<sub>2</sub>. *J. Mater. Chem.* **2012**, *22*, 11364–11369.
- (13) Watson, D. F.; Meyer, G. J. Cation Effects in Nanocrystalline Solar Cells. *Coord. Chem. Rev.* **2004**, *248*, 1391–1406.
- (14) Davis, V. K.; Sampaio, R. N.; Marquard, S. L.; Meyer, G. J. Electric Fields Detected on Dye-Sensitized TiO<sub>2</sub> Interfaces: Influence of Electrolyte Composition and Ruthenium Polypyridyl Anchoring Group Type. *J. Phys. Chem. C* **2018**, *122*, 12712–12722.
- (15) Wei, L.; Jiang, L.; Yuan, S.; Ren, X.; Zhao, Y.; Wang, Z.; Zhang, M.; Shi, L.; Li, D. Valence Band Edge Shifts and Charge-transfer Dynamics in Li-Doped NiO Based p-type DSSCs. *Electrochim. Acta* **2016**, *188*, 309–316.
- (16) Dini, D.; Halpin, Y.; Vos, J. G.; Gibson, E. A. The Influence of the Preparation Method of NiOx Photocathodes on the Efficiency of P-Type Dye-Sensitized Solar Cells. *Coord. Chem. Rev.* **2015**, *304–305*, 179–201.
- (17) Wood, C. J.; Summers, G. H.; Clark, C. A.; Kaeffer, N.; Braeutigam, M.; Carbone, L. R.; D'Amario, L.; Fan, K.; Farré, Y.; Narbey, S.; Oswald, F.; Stevens, L. A.; Parmenter, C. D. J.; Fay, M. W.; La Torre, A.; Snape, C. E.; Dietzek, B.; Dini, D.; Hammarström, L.; Pellegrin, Y.; Odobel, F.; Sun, L.; Artero, V.; Gibson, E. A. A Comprehensive Comparison of Dye-Sensitized NiO Photocathodes for Solar Energy Conversion. *Phys. Chem. Chem. Phys.* **2016**, *18*, 10727–10738.
- (18) Click, K. A.; Beauchamp, D. R.; Garrett, B. R.; Huang, Z.; Hadad, C. M.; Wu, Y. A Double-Acceptor as a Superior Organic Dye Design for P-Type DSSCs: High Photocurrents and the Observed Light Soaking Effect. *Phys. Chem. Chem. Phys.* **2014**, *16*, 26103–26111.
- (19) Gibson, E. A.; Smeigh, A. L.; Le Pleux, L.; Fortage, J.; Boschloo, G.; Blart, E.; Pellegrin, Y.; Odobel, F.; Hagfeldt, A.; Hammarström, L. A p-Type NiO-Based Dye-Sensitized Solar Cell with an Open-Circuit Voltage of 0.35 V. *Angew. Chem., Int. Ed.* **2009**, *48*, 4402–4405.
- (20) Giribabu, L.; Bolligarla, R.; Panigrahi, M. Recent Advances of Cobalt(II/III) Redox Couples for Dye-Sensitized Solar Cell Applications. *Chem. Rec.* **2015**, *15*, 760–788.
- (21) Redmond, G.; Fitzmaurice, D. Spectroscopic Determination of Flatband Potentials for Polycrystalline Titania Electrodes in Non-aqueous Solvents. *J. Phys. Chem.* **1993**, *97*, 1426–1430.
- (22) Wang, H.; Peter, L. M. Influence of Electrolyte Cations on Electron Transport and Electron Transfer in Dye-Sensitized Solar Cells. *J. Phys. Chem. C* **2012**, *116*, 10468–10475.
- (23) Jeanbourquin, X. A.; Li, X.; Law, C.; Barnes, P. R. F.; Humphry-Baker, R.; Lund, P.; Asghar, M. I.; O'Regan, B. C. Rediscovering a Key Interface in Dye-Sensitized Solar Cells: Guanidinium and Iodine Competition for Binding Sites at the Dye/Electrolyte Surface. *J. Am. Chem. Soc.* **2014**, *136*, 7286–7294.
- (24) Fredin, K.; Nissfolk, J.; Boschloo, G.; Hagfeldt, A. The Influence of Cations on Charge Accumulation in Dye-Sensitized Solar Cells. *J. Electroanal. Chem.* **2007**, *609*, 55–60.
- (25) Liu, Y.; Hagfeldt, A.; Xiao, X.-R.; Lindquist, S.-E. Investigation of Influence of Redox Species on the Interfacial Energetics of a Dye-Sensitized Nanoporous TiO<sub>2</sub> Solar Cell. *Sol. Energy Mater. Sol. Cells* **1998**, *55*, 267–281.
- (26) Walter, M. G.; Warren, E. L.; McKone, J. R.; Boettcher, S. W.; Mi, Q.; Santori, E. A.; Lewis, N. S. Solar Water Splitting Cells. *Chem. Rev.* **2010**, *110*, 6446–6473.
- (27) Lyon, L. A.; Hupp, J. T. Energetics of Semiconductor Electrode/Solution Interfaces: EQCM Evidence for Charge-Compensating Cation Adsorption and Intercalation during Accumulation Layer Formation in the Titanium Dioxide/Acetonitrile System. *J. Phys. Chem.* **1995**, *99*, 15718–15720.
- (28) Liu, H.; Xiang, W.; Tao, H. Probing the Influence of Lithium Cation as Electrolyte Additive for the Improved Performance of P-Type Aqueous Dye Sensitized Solar Cells. *J. Photochem. Photobiol., A* **2017**, *344*, 199–205.
- (29) Boschloo, G.; Hagfeldt, A. Spectroelectrochemistry of Nanostructured NiO. *J. Phys. Chem. B* **2001**, *105*, 3039–3044.
- (30) D'Amario, L.; Boschloo, G.; Hagfeldt, A.; Hammarström, L. Tuning of Conductivity and Density of States of NiO Mesoporous Films Used in p-Type DSSCs. *J. Phys. Chem. C* **2014**, *118*, 19556–19564.
- (31) Marrani, A. G.; Novelli, V.; Sheehan, S.; Dowling, D. P.; Dini, D. Probing the Redox States at the Surface of Electroactive Nanoporous NiO Thin Films. *ACS Appl. Mater. Interfaces* **2014**, *6*, 143–152.
- (32) D'Amario, L.; Jiang, R.; Cappel, U. B.; Gibson, E. A.; Boschloo, G.; Rensmo, H.; Sun, L.; Hammarström, L.; Tian, H. Chemical and Physical Reduction of High Valence Ni States in Mesoporous NiO Film for Solar Cell Application. *ACS Appl. Mater. Interfaces* **2017**, *9*, 33470–33477.
- (33) D'Amario, L.; Antila, L. J.; Pettersson Rimgard, B.; Boschloo, G.; Hammarström, L. Kinetic Evidence of Two Pathways for Charge Recombination in NiO-Based Dye-Sensitized Solar Cells. *J. Phys. Chem. Lett.* **2015**, *6*, 779–783.

(34) D'Amario, L.; Föhlinger, J.; Boschloo, G.; Hammarström, L. Unveiling Hole Trapping and Surface Dynamics of NiO Nanoparticles. *Chem. Sci.* **2018**, *9*, 223–230.

(35) Zhu, H.; Hagfeldt, A.; Boschloo, G. Photoelectrochemistry of Mesoporous NiO Electrodes in Iodide/Triiodide Electrolytes. *J. Phys. Chem. C* **2007**, *111*, 17455–17458.

(36) Boschloo, G.; Hagfeldt, A. Characteristics of the Iodide/Triiodide Redox Mediator in Dye-Sensitized Solar Cells. *Acc. Chem. Res.* **2009**, *42*, 1819–1826.

(37) Nelson, J. J.; Amick, T. J.; Elliott, C. M. Mass Transport of Polypyridyl Cobalt Complexes in Dye-Sensitized Solar Cells with Mesoporous TiO<sub>2</sub> Photoanodes. *J. Phys. Chem. C* **2008**, *112*, 18255–18263.

(38) Ito, S.; Murakami, T. N.; Comte, P.; Liska, P.; Grätzel, C.; Nazeeruddin, M. K.; Grätzel, M. Fabrication of Thin Film Dye Sensitized Solar Cells with Solar to Electric Power Conversion Efficiency over 10%. *Thin Solid Films* **2008**, *516*, 4613–4619.

(39) Gelderman, K.; Lee, L.; Donne, S. W. Flat-Band Potential of a Semiconductor: Using the Mott–Schottky Equation. *J. Chem. Educ.* **2007**, *84*, 685.

(40) Shannon, R. Revised Effective Ionic Radii and Systematic Studies of Interatomic Distances in Halides and Chalcogenides. *Acta Crystallogr., Sect. A: Cryst. Phys., Diffraction, Theor. Gen. Crystallogr.* **1976**, *32*, 751–767.

(41) Uehara, S.; Sumikura, S.; Suzuki, E.; Mori, S. Retardation of Electron Injection at NiO/Dye/Electrolyte Interface by Aluminium Alkoxide Treatment. *Energy Environ. Sci.* **2010**, *3*, 641–644.

(42) Flynn, C. J.; McCullough, S. M.; Oh, E.; Li, L.; Mercado, C. C.; Farnum, B. H.; Li, W.; Donley, C. L.; You, W.; Nozik, A. J.; McBride, J. R.; Meyer, T. J.; Kanai, Y.; Cahoon, J. F. Site-Selective Passivation of Defects in NiO Solar Photocathodes by Targeted Atomic Deposition. *ACS Appl. Mater. Interfaces* **2016**, *8*, 4754–4761.

(43) Huang, Z.; Natu, G.; Ji, Z.; Hasin, P.; Wu, Y. P-Type Dye-Sensitized NiO Solar Cells: A Study by Electrochemical Impedance Spectroscopy. *J. Phys. Chem. C* **2011**, *115*, 25109–25114.

(44) Wang, Q.; Moser, J.-E.; Grätzel, M. Electrochemical Impedance Spectroscopic Analysis of Dye-Sensitized Solar Cells. *J. Phys. Chem. B* **2005**, *109*, 14945–14953.

(45) Gillmeister, K.; Kiel, M.; Widdra, W. Image Potential States at Transition Metal Oxide Surfaces: A Time-Resolved Two-Photon Photoemission Study on Ultrathin NiO Films. *Phys. Rev. B: Condens. Matter Mater. Phys.* **2018**, *97*, 085424.

(46) Bisquert, J.; Fabregat-Santiago, F.; Mora-Seró, I.; Garcia-Belmonte, G.; Giménez, S. Electron Lifetime in Dye-Sensitized Solar Cells: Theory and Interpretation of Measurements. *J. Phys. Chem. C* **2009**, *113*, 17278–17290.

(47) Bisquert, J.; Marcus, R. A. Device Modeling of Dye-Sensitized Solar Cells. In *Multiscale Modelling of Organic and Hybrid Photovoltaics*; Beljonne, D., Cornil, J., Eds.; Springer: Berlin, 2014; pp 325–395.